Electrosorption-Induced Deformation of Nanoporous Carbons: Solvation Pressure from Molecular Dynamics and Continuum Theory

Andrei L. Kolesnikov,[†] Patrick Huber,[‡,¶] Michael Fröba,[§] and Gennady Y. Gor[*,†]

[†]*Otto H. York Department of Chemical and Materials Engineering, New Jersey Institute of Technology, Newark, New Jersey 07102, United States*

[‡]*Institute for Materials and X-ray Physics, Hamburg University of Technology, 21073 Hamburg, Germany*

[¶]*Center for X-ray and Nano Science, Deutsches Elektronen-Synchrotron, 22607 Hamburg, Germany*

[§]*Institute of Inorganic and Applied Chemistry, University of Hamburg, Hamburg 20146, Germany*

E-mail: gor@njit.edu

Abstract

Nanoporous carbons play an important role in different electrochemical applications such as being utilized as electrodes in supercapacitors. Application of electric potential to a porous electrode in electrolyte solution stimulates adsorption or desorption of ions on the electrode surface. Electrosorption causes appearance of solvation pressure in the pores and results in electrode deformation. In this work, using molecular dynamics simulations and the continuum theory based on the modified Poisson-Boltzmann equation, we studied the structure of the electrical double layer in slit graphitic micropores

filled with a NaCl aqueous solution, and solvation pressure in these pores. We focused on the behavior of the solvation pressure as a function of pore width and surface charge density. Within molecular dynamics simulations, two different water models were used – an explicit model based on SPC/E water molecules and an implicit model, i.e., structureless background with fixed dielectric permittivity. The latter allows us to relate molecular dynamics simulation to the continuum theory. Simulations with explicit water show a qualitatively different behavior of the solvation pressure in the 1 and 2 nm pores as a function of the surface charge density. We demonstrated that the value of the solvation pressure is defined by a delicate balance between Van der Waals and electrostatic contributions. We demonstrated that the theory predicts the dependence of the solvation pressure on the pore width, which matches the results of simulations using the implicit water model. Finally, we adapted the continuum theory, developed for adsorption-induced deformation to estimate the deformation of a carbon electrode due to electrosorption. Our results can be used in the further development of nanoporous actuators working based on electrosorption-induced deformation.

Introduction

Application of electric potential to a porous electrode in electrolyte solution, stimulates adsorption or desorption of ions on the electrode surface. This electrosorption process is behind the mechanism of energy storage in supercapacitors. Since the early works on electrosorption in porous carbons,[1,2] electrosorption showed to be accompanied with deformation. On the one hand, for energy storage devices, these deformations are obviously undesired.[3,4] On the other hand, electrosorption-induced deformation offers the potential to build new types of actuators,[5] which operate at exceptionally low operating voltages,[6] a fraction of a volt compared to classical piezoelectric materials, which typically require several hundred volts. This is particularly interesting for biological applications. Mechanical forces play a crucial role in shaping biological systems, influencing the growth, structure and functionality of various living tissues.[7–10] Research has shown that mechanical stimuli can induce significant changes in cellular morphology, signalling pathways and gene expression through the activation of specialised mechanoreceptors such as piezo channels. The unique combination of mechanical force generation and low operating voltages offered by nanoporous electrodes opens up exciting possibilities in the field of biomedical engineering. These materials could be integrated into medical surfaces and implants, allowing precise electrically controlled manipulation of tissues[10] and even interfacing with brain function, i.e. neuronal activity.[11]

The first actuators based on electrosorption-induced deformation utilized carbon nanotubes,[5] followed by those made of nanoporous metals.[12,13] Advancements in sol-gel synthesis of templated monolithic carbons helped further advancing such actuators.[14] These materials can be prepared with precise control of the pore sizes, as well as, surface and mechanical properties. Further development of such materials to use them as actuators can benefit from a model capable of predicting the dependence of electrosorption-induced strains on these materials properties. This work aims to take steps towards building such a model.

Electrosorption-induced deformation is driven mainly by solvation pressure in the pores,[15] which has been studied theoretically in a number of works, e.g.[3,16–18] The simplest, contin-

uum approach based on the Poisson-Boltzmann equation[19] predicts the quadratic dependence of the solvation pressure on the surface charge density. This is indeed consistent with multiple experimental studies,[4,14,20,21] and with more sophisticated theoretical approaches. Recently, a modified Poisson-Boltzmann (mPB) model[22] was used to explain the complex electrosorption-induced deformation of CMK-3.[14] In addition to continuum models, a number of molecular simulation studies focused on solvation pressure resulting from electrosorption in carbon nanopores. In Refs.[20,23] molecular dynamics (MD) was applied to study the behavior of room-temperature ionic liquids in micro- and mesopores, showing the parabolic-like behavior of pressure in 1.2 nm and 7 nm pore as a function of charge density.[20] In paper[23] the focus was shifted toward pore size dependence of the solvation pressure at fixed surface charge densities. Several publications investigated the solvation pressure of confined aqueous electrolytes as a function of surface charge density and pore size.[24–29] In Ref.[24] a "primitive" model was used to calculate contour maps demonstrating attracto-repulsive regimes of wall interactions. In Ref.[25] the authors applied the Monte Carlo method to study interactions between charged surfaces. They demonstrated that the additivity of hydration and electrostatic solvation pressure contributions breaks down even at moderate surface charges. This was partially attributed to the possible modification of the hydration force due to surface-charge-induced water reorientation. In Ref.[27] the water-mediated interactions between calcium carbonate surfaces were studied as a function of the surface separations. In paper[29] the authors studied dense electrolytes using a combination of molecular dynamics, Monte Carlo simulation and classical density functional theory (cDFT). One of the findings was that ion-surface and ion-ion excluded-volume correlations are important for a correct description of the solvation pressure and ion density profiles of highly concentrated electrolytes ($> 1\,\mathrm{M}$).

To summarize, these papers mainly consider the dependence of the solvation pressure on the distance between charged surfaces using the surface charge density as a parameter. While focusing on the solvation pressure, they lack the transition to the description of

electrosorption-induced deformation. Therefore, study of the surface charge dependence of the solvation pressure and its generalization to the macroscale is still needed. In the current paper, we study the behavior of the solvation pressure in slit carbon micropores immersed in NaCl aqueous solution as a function of surface charge density. We used three different theoretical approaches: (1) molecular dynamics (MD) simulations with explicit water, (2) MD simulations with implicit water, (3) continuum model based on the modified Poisson-Boltzmann model. These models help clarify the role of individual force contributions to the calculated solvation pressure. We used implicit solvent molecular dynamics to verify our mPB model, which was further used to predict the electrosorption-induced deformation on the macroscopic scale with account of the possible pore size distribution.

Methods

In this work, we describe an electrosorption process on one-pore scale using three different theoretical approaches: classical molecular dynamics with implicit and explicit water and the modified Poisson-Boltzmann equation. The main goal of our study is to calculate solvation pressure as a function of pore width and surface charge density. Two types of water models are used in our simulations: SPC/E[30] and water as an implicit solvent, i.e., a structureless background with constant dielectric permittivity. The latter allows us to perform an almost direct comparison of the MD results with the results obtained within the framework of the modified Poisson-Boltzmann equation. In this section, we describe the model and simulation procedure in detail. The model will be further extended and used in the **Discussion** section to apply calculations on the pore scale to predict the macroscopic deformation of microporous carbons caused by electrosorption.

Molecular Dynamics Simulations

We studied the electrosorption of NaCl solution using classical molecular dynamics in the canonical (NVT) ensemble with a constant number of particles (N), volume (V) and temperature (T). The temperature was fixed at 298.15 K by applying the Nose-Hoover thermostat. We represent the pores by two carbon walls consisting of five graphene sheets each (see Fig. 1). We considered two pore widths (denoted by H), namely 1 nm and 2 nm. The rectangular simulation box with 9.5 nm side lengths along the x and z axes and 4.181 18 nm side length along the y axis was used. The pores were immersed in an aqueous sodium chloride solution. During the charging process, additional partial charges of the same sign were assigned to the inner graphene sheets of both pore walls. We introduced additional salt ions to compensate for the pore charge and make the simulation box electrically neutral.

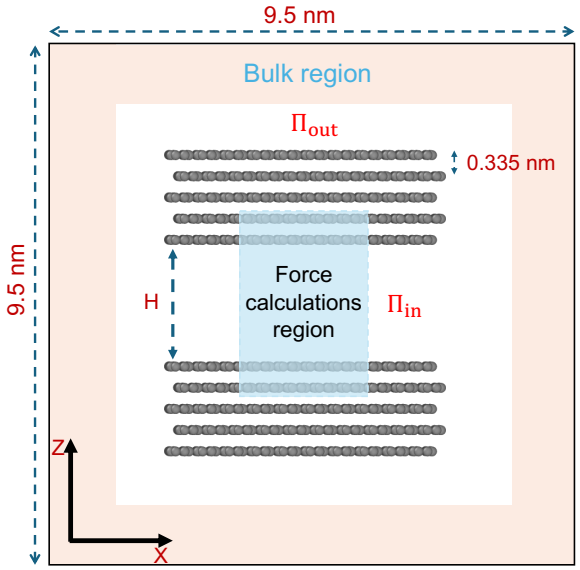

Figure 1: Empty simulation box used in the NVT molecular dynamics to estimate the solvation pressure. We denoted regions where we calculated the corresponding bulk density and the Π_{in} in the pore by colors.

In the current work, we used implicit and explicit water models. The implicit water was simulated as a structureless medium with relative dielectric permittivity $\varepsilon = 78$.[31] The

ion-ion short-range interactions were described via (WCA)[32] potential:

$$u(r) = \begin{cases} u_{\mathrm{LJ}}(r) + \epsilon & r < 2^{1/6}\sigma \\ 0 & r > 2^{1/6}\sigma \end{cases} \tag{1}$$

where $u_{\mathrm{LJ}}(r)$, ϵ and σ are the Lennard-Jones potential and its parameters from MD simulations with explicit water. In the following, we will denote implicit water simulations as MD/WCA and the simulations with explicit water as MD/SPCE for the sake of shortening. There are no further differences in the simulation procedure between two types of solvents, so we will continue with the description of the explicit water, stating that the same is true for the MD/WCA. We used the SPC/E water model,[30] as an explicit solvent model with parameters for ion-ion interactions taken from Ref.[33] The interaction parameters are summarized in Table 1. We used the Lorentz-Berthelot combining rule and cutoff equal to 0.9 nm. No shifting or tail corrections were applied. The SHAKE algorithm was used to constrain the water molecule bond and bend degrees of freedom. The integration time step was chosen as 1 fs. The total simulation length was separated into equilibration and production parts – the former was 8 ns, the latter was 40 ns. The example input files are included as the Supplementary Materials.

Table 1: Parameters for intermolecular potentials. The value in brackets correspond to the MD/WCA simulations.

Atom type	σ / nm	ϵ / kcal/mol	q / e	References
O	0.3165	0.15539	-0.8476	[30]
H	-	-	0.4238	[30]
Na^+	0.235	0.13 (0.1)	1	[33, 34]
Cl^-	0.44	0.1	-1	[33, 34]
C	0.34	0.0557	0	[35]

The solvation pressure was calculated as a difference between the pressures on the inner

and the outer graphene sheets (see Fig. 1):

$$\Delta\Pi = \Pi_{\text{in}} - \Pi_{\text{out}}, \tag{2}$$

where Π_{in} is the inner pressure and Π_{out} is the outer pressure. We calculated the pressures by adding the forces on the individual carbon atoms and dividing the total force by the area occupied by the atoms. To do it, we used only the middle part of the pore excluding the atoms that were less than 1 nm from the pore edge along the x-axis (see Fig. 1). The same region width was used to calculate the outer pressure.

In addition to the simulations in the NVT ensemble, we also performed the simulations in the isothermal-isobaric (NPT) ensemble to estimate the bulk pressure dependence on the density and ion concentration. Using the SPC/E water model, we calculated the bulk densities of the aqueous NaCl solution at a fixed number of particles, pressure (P), and temperature. The pressure was fixed at 1 atm using a Nose-Hoover barostat. We used 800 water molecules and different numbers of ion pairs (from 0 to 25). The simulations were 25 ns long and the density was calculated using the last 20 ns. For the MD/WCA model we used 200 ion pairs to estimate the bulk pressures at different molarities. The total simulation length was 25 ns and the last 15 ns were used as a production run.

Modified Poisson-Boltzmann equation

To compare our simulation results with theoretical predictions, we consider a slit pore of width H immersed in the electrolyte solution. We assume that the pore is sufficiently long that we can use a one-dimensional problem formulation. The pore walls carry the homogeneous surface charge with density ξ. The solvent is treated as a structureless background with relative dielectric permittivity ε. The classical Poisson-Boltzmann equation describes the distribution of electric potential and point charges in the solution. The framework of a modified Poisson-Boltzmann equation allows us to include additional interactions to the

model.[22,36,37] In this work, we include the steric interaction between ions, considering them as charged hard spheres, and short-range interactions with the pore walls. The resulting equations describing the distribution of electrostatic potential ($\psi = \psi(z)$) and ion concentrations ($c_\pm = c_\pm(z)$) are:

$$\varepsilon\varepsilon_0 \frac{\mathrm{d}^2\psi}{\mathrm{d}z^2} = -q(c_+ - c_-) \tag{3}$$

$$\mu_0(c_{0,\pm}) = \mu_{\mathrm{id}}(c_\pm) + \mu_{\mathrm{hs}}(c_\pm) \pm q\psi + V_{\mathrm{ext}}(z) + V_{\mathrm{ext}}(H - z), \tag{4}$$

with the external ion-wall short range potential having the form:[38,39]

$$V_{\mathrm{ext}}(z) = 2\pi\rho_{\mathrm{s}}\sigma_{\mathrm{sf}}^2\epsilon_{\mathrm{sf}}\left[\frac{2}{5}\left(\frac{\sigma_{\mathrm{sf}}}{z}\right)^{10} - \left(\frac{\sigma_{\mathrm{sf}}}{z}\right)^{4}\right]. \tag{5}$$

Eq. 5 represents the interaction of the molecule with a surface having the areal density ρ_{s} of the interaction sites. Here, σ_{sf} and ϵ_{sf} are the Lennard-Jones parameters of interactions between the guest molecule and the surface particle; ε_0 is the vacuum dielectric permittivity; c_+ and c_- are cation and anion concentrations; $\mu_{\mathrm{id}}(c_\pm)$ and $\mu_{\mathrm{hs}}(c_\pm)$ are the ideal and steric contribution to the chemical potential; $\mu_0(c_{0,\pm})$ is the bulk chemical potential of the ions. The excess chemical potentials were obtained in the bulk limit of the fundamental measure theory,[40,41] which corresponds to the Perkus-Yevick approximation in the one-component case. We refer the reader to the existing literature that provides formulations for the chemical potentials and pressure.[19,37,41] Solving this system of equations (3 and 4) one can obtain the profile of electrostatic potential and ion concentrations. The effective diameters of the hard spheres were determined by hybrid Barker-Henderson rule:[19,42]

$$d_\pm = \int_0^{2^{1/6}\sigma_\pm} \left[1 - \exp\left(-\frac{u(r)_\pm}{k_{\mathrm{B}}T}\right)\right]\mathrm{d}r, \tag{6}$$

where $u(r)_\pm$ is the WCA potential of interactions Eq. 1.

The pressure inside the pore in this system can be written in the following form:[37]

$$\Pi_{\mathrm{in}} = -\sum_{\mathrm{i}=\pm} \int_0^H c_{\mathrm{i}} \frac{\mathrm{d}V_{\mathrm{ext}}}{\mathrm{d}z} \mathrm{d}z - \frac{\varepsilon\varepsilon_0}{2} \left(\frac{\mathrm{d}\psi}{\mathrm{d}z} \right)^2, \tag{7}$$

where the first term quantifies the short-range interactions between pore walls and the second term the long-range (electrostatic) interactions. Thus, the pressure (Eq. 7) can be calculated from the solution of Eqs. 3 and 4.

Results

We performed calculations of the density of the aqueous solution of sodium chloride as a function of molarity. The results are shown in Fig. 2. We estimate that the density at 1 mol/l is 1.026 g/cm^3 using the linear fit of the MD results obtained in the NPT ensemble. This value is used as a reference in our calculations of the solvation pressure.

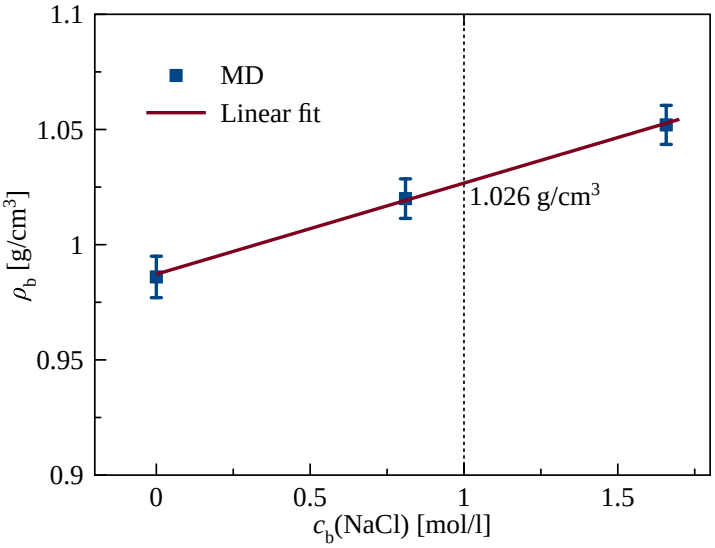

Figure 2: Density of the aqueous electrolyte solution as a function of NaCl molarity. The points are the results of our MD calculations in NPT ensemble and the line is the linear fit used to interpolate the MD results.

To setup the simulation of the pore, we first estimate the number of water molecules and

ion pairs we need to obtain similarly to the bulk values of density and molarity in the NVT box far from the pore. This region is denoted as "bulk region" in Fig. 1. These preliminary estimations were performed in the same NVT box with a 3 nm pore. The simulation boxes with 1 and 2 nm pores can be considered as a result of the process of reducing the distance between the pore walls from 3 nm occurring in the same environment, i.e. volume, number of water molecules and temperature are fixed. We adjusted the number of ions to maintain overall electroneutrality, relating the surface pore charge density and the number of added ions to the system. So, the total number of water molecules was fixed at 10100, the amount of sodium chloride ions in the simulations is summarized in Table 2. The chosen surface charge densities are given in Table 2, and cover a range similar to that used in.[25]

Table 2: Number of ions in the simulations with different surface charge densities (ξ).

Surface charge (ξ) / μC/cm^2	Na^+	Cl^-
-23.7	221	170
-15.8	204	170
-7.9	170	187
0	170	170
7.9	170	187
15.8	170	204
23.7	170	221

Fig. 3 shows the concentration profiles at three different surface charges ($-23.7\,\mu$C/cm^2, 0 and $23.7\,\mu$C/cm^2) for both the 1 and 2 nm pores. The ions and water concentrations corresponding to positive and negative surface charges are different from those in the vicinity of the neutral surface. When the surface is negatively charged, water molecules are partially oriented and directed by hydrogens to the surface, also the first oxygen peak becomes narrower compared to those at $\xi = 0$. Additionally, cations repel hydrogens, and anions are almost absent in the pore. We observe different concentration profiles for positively charged surfaces – hydrogens are turned away from the surface and attracted to the anions. At both surface charges, electric double layer formation also leads to narrowing of the first oxygen peak, which should inevitably impact the solvation pressure.

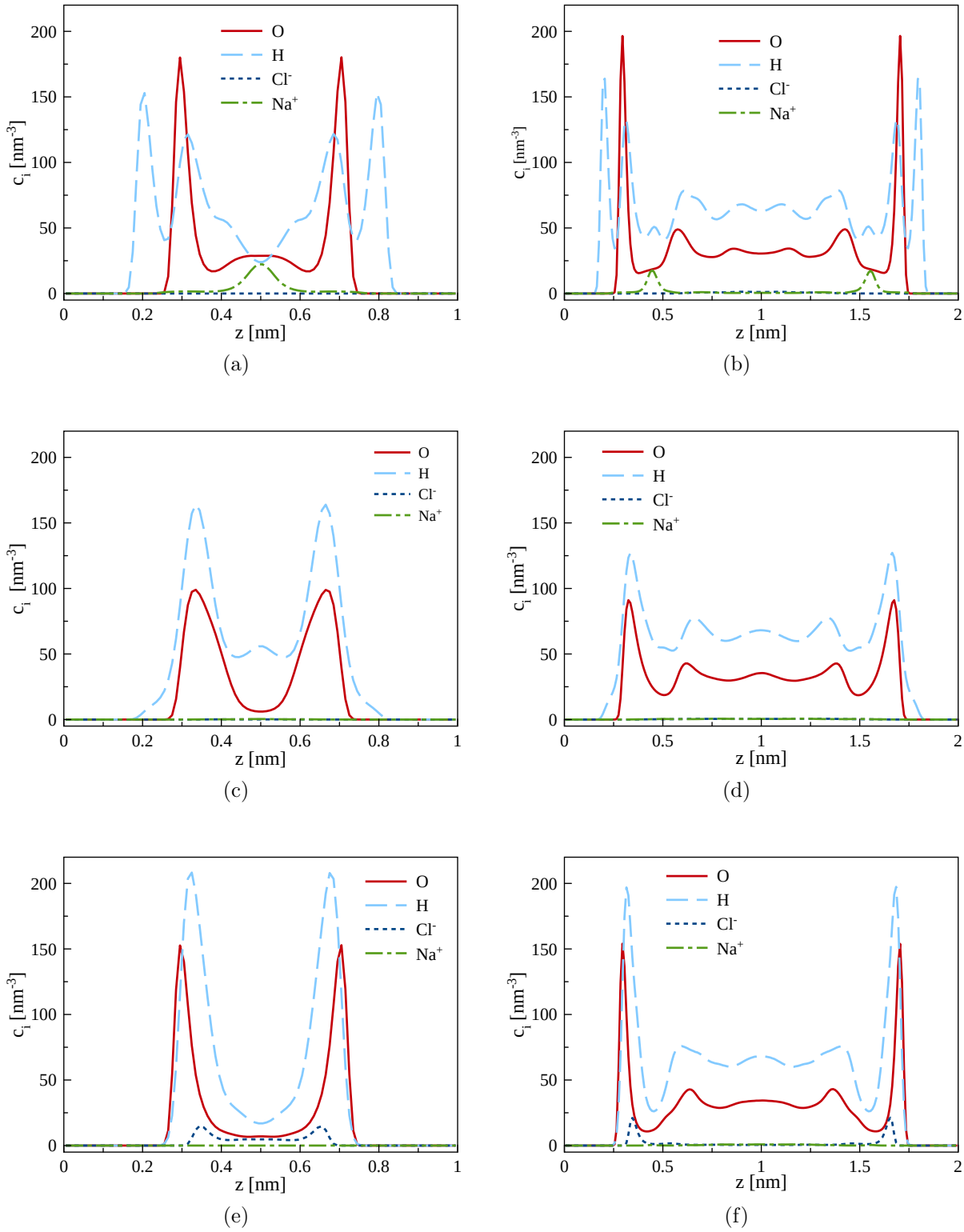

Figure 3: Concentration profiles in 1 nm (left column) and 2 nm (right column) pores; (a) and (b) correspond to surface charge density of $-23.7\,\mu C/cm^2$; (c) and (d) correspond to surface charge density of $0\,\mu C/cm^2$; (e) and (f) correspond to surface charge density of $23.7\,\mu C/cm^2$.

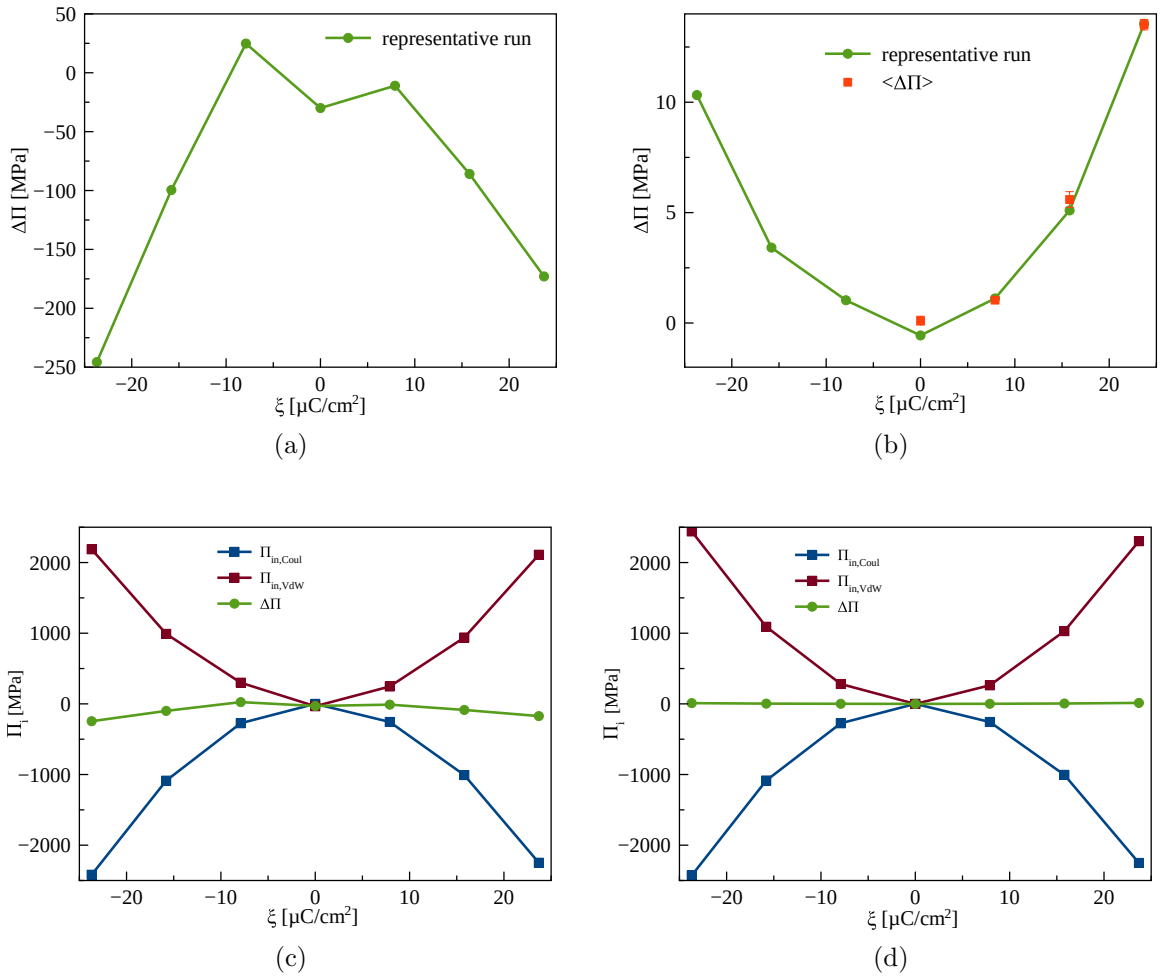

Figure 4: Solvation pressure calculated from MD simulations with explicit water model. (a) Solvation pressure in 1 nm pore; (b) Solvation pressure in 2 nm pore; $\langle\Pi\rangle$ denote an average over 5 independent runs; (c) VdW and electrostatic contributions for solvation pressure in 1 nm pore; (d) VdW and electrostatic contributions for solvation pressure in 2 nm pore.

Fig. 4 presents the solvation pressure calculated in 1 nm and 2 nm pores as a function of the surface charge density, showing qualitatively different behavior. $\Delta\Pi$ in the 1 nm pore is a concave down roughly parabolic function with some non-monotonic behavior at low ξ. On the other hand $\Delta\Pi$ in 2 nm is a concave up and slightly asymmetric parabolic function. The solvation pressure in the 1 nm pore is also different in magnitude being approximately 10 times greater than in the 2 nm pore. For both 1 nm and 2 nm pores, the solvation pressure as a function of ξ can be split into two contributions, one originating from short-range (VdW)

interactions and the other from long-range (electrostatic) interactions. Both contributions have a parabolic shape as a function of ξ, and the resulting behavior of the solvation pressure depends on the fine balance between them, as shown in Figs. 4c and 4d.

The balance between short-range and long-range contributions to the electrosorption-induced solvation pressure can be further investigated by means of MD/WCA simulations and the mPB approach. In the MD/WCA simulations, we used the same number of ions as was determined for SPC/E water, and summarized in Table 2. In MD/WCA simulations we obtained a molarity approximately equal to 0.8 M. The same value was used in our theoretical calculations using the mPB model as well as the same LJ interaction parameters. Fig. 5a presents Π_{in} as a function of pore width demonstrating good agreement between the theoretical predictions and the results of MD/WCA simulations. The calculations were performed in the system with zero surface charge density. Both MD and the model demonstrate the same oscillatory behavior with one pronounced maximum at $H \approx 0.7\,\text{nm}$ and the minimum at $H \simeq 1\,\text{nm}$.

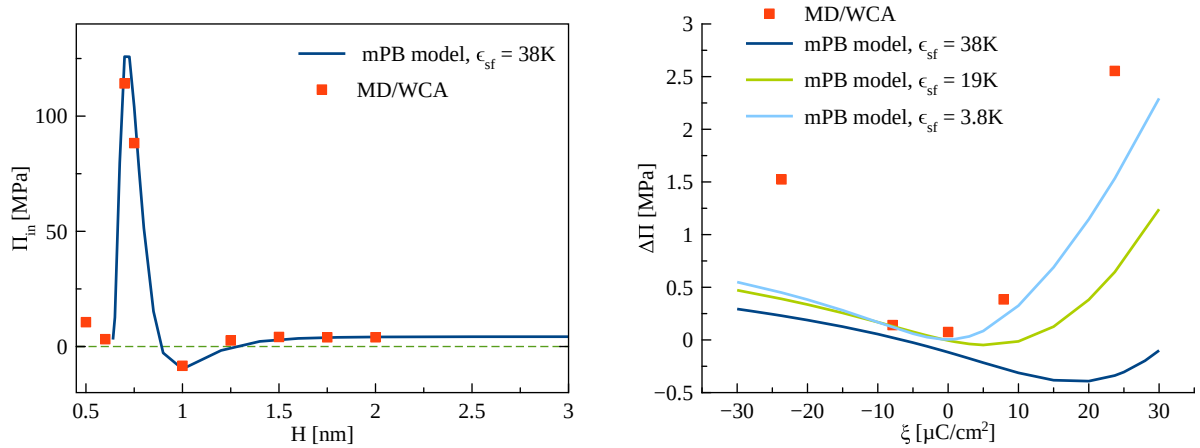

Figure 5: (a) Electrosorption pressure in the pores at $\xi = 0$ as a function of pore size; (b) Electrosorption-induced solvation pressure in 2 nm pore. The symbols represent MD/WCA results with implicit water and lines are the results of the model. From MD/WCA simulations we obtained molality $\approx 0.8\,\text{M}$ and used this value in theoretical calculations. The value of $\epsilon_{\text{sf}} = 38\,\text{K}$ corresponds to the one used in molecular dynamics.

Fig. 5b shows the solvation pressure calculated for 2 nm pore as a function of the surface charge density. The solvation pressure predicted by MD/WCA has a minimum at $\xi = 0$ and demonstrate asymmetry, due to the difference in the size of the ions. Fig. 5b shows an appreciable deviation of the predictions of the mPB model from the MD/WCA results when $\epsilon_{sf} = 38\,\mathrm{K}$ are used in both. However, if ϵ_{sf} is treated as an adjustable parameter within the mPB model, the agreement with MD/WCA results can be made satisfactory. This suggests that the mPB model overestimated the effect of the external field on the eletrosorption process. Also, an increase of the energetic parameter leads to a shift of the minimum solvation pressure on the mPB model results. Further, we can compare the Van der Waals and electrostatic contributions obtained from the mPB model and molecular dynamics. The results are presented in Fig. 6 for $\epsilon_{sf} = 38\,\mathrm{K}$. Here, the MD/WCA and mPB approaches demonstrate similar parabolic shapes for both contributions. Also, as was in the MD/SPCE, the short-range part is positive and the electrostatic one is negative. So, the same conclusion can be made, that is, $\Delta\Pi$ is defined by the balance between them, and can take both positive and negative values.

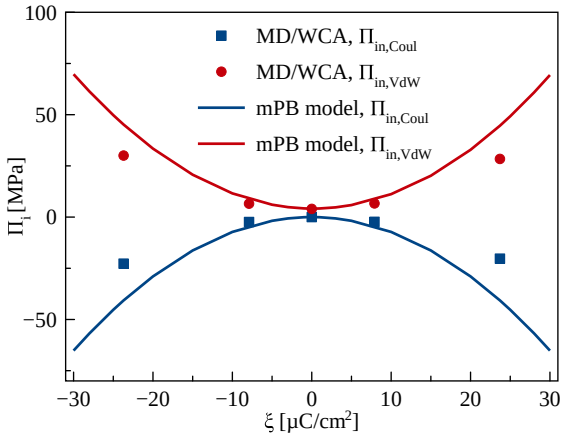

Figure 6: VdW and electrostatic contributions for solvation pressure, calculated using MD/WCA and mPB model for 2 nm pore. The theoretical results are obtained with $\epsilon_{sf} = 38\,\mathrm{K}$ in in 2 nm pore.

Figure 7 shows the ion concentration profiles calculated in the 2 nm pore at $\xi = -23.7$ and $23.7\,\mu\mathrm{C/cm^2}$ for various ϵ_{sf} using MD/WCA and mPB model. The theoretical con-

centration profiles calculated for the negatively charged pore match the MD/WCA results quantitatively, while for the positively charged pore, only qualitative agreement is observed.

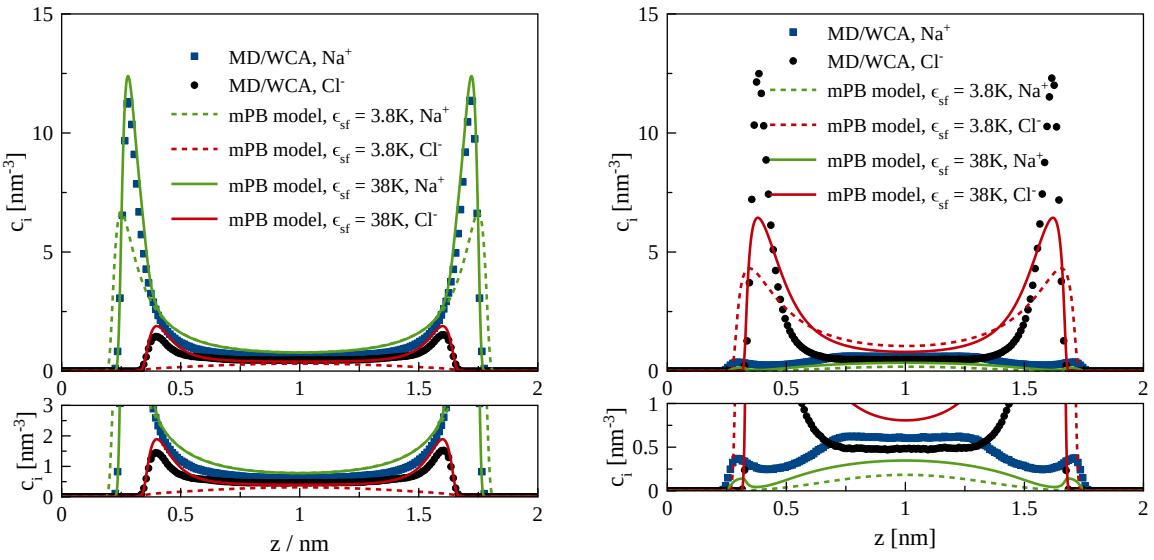

(a) (b)

Figure 7: Ion concentration profiles in 2 nm pore predicted by MD/WCA and mPB model: (a) corresponds to surface charge density of $-23.7\,\mu\mathrm{C/cm^2}$; (b) corresponds to surface charge density of $23.7\,\mu\mathrm{C/cm^2}$. The markers correspond to the MD/WCA simulation results; the solid lines correspond to the model results with $\epsilon_{\mathrm{sf}} = 38\,\mathrm{K}$; the dotted lines correspond to the model results with $\epsilon_{\mathrm{sf}} = 3.8\,\mathrm{K}$.

Discussion

In Figure 7 we compared the MC/WCA ion concentrations and the model predictions and demonstrated that the profiles calculated using $\epsilon_{\mathrm{sf}} = 38\,\mathrm{K}$ better match the simulation results at a negative surface charge density. Most probably, it is due to the difference in ion sizes, Na^+ (approx. 0.235 nm) is almost twice smaller than Cl^-. It is not surprising that our local model can adequately describe cation distributions since our equations should be more and more precise with the decrease of ion diameters and concentrations. In turn, positively charged carbon walls will increase the attraction of anions, whose diameters are approximately equal to 0.4 nm. At high concentrations near to the solid walls, our local model fails to predict the

distribution of the bulky ions and a the model accounting for nonlocal ion-ion interactions is required to obtain quantitative agreement with the simulation results.

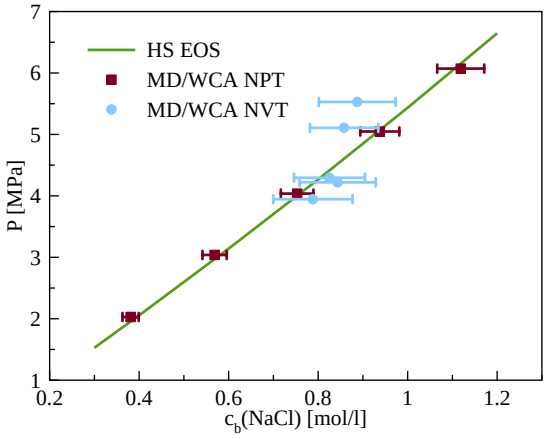

Figure 8: Pressure at different electrolyte molarities calculated using MD/WCA within NPT and NVT ensembles. The line is the results of the Percus-Yevick equation of state which arise within our model; the dots are the results from molecular dynamics.

The change in solvation pressure with the increase of the surface charge density is mainly due to the change in Π_{in}, however, the bulk pressure Π_{out} appears to also increase. To investigate this effect in more detail, we compared it with a bulk pressure calculated in the NPT simulation (see **Model** section) in MD/WCA case. Additionally, in Fig. 8 we also add the result of the equation of state corresponding to the chemical potential in Eq. 4. The results from NVT simulations follow a similar trend compared with those from NPT ones. It suggests that the pressure may vary due to the change in the number of ions in the simulation box (see Table 2). Another possible reason is the interactions between surface charges and the ions in the bulk region leading to a slight change in the ion concentration profiles.

Knowing the concentration profiles also allows us to estimate the forces acting on the pore walls. We can do this using several simplifying assumptions: water and ion interact with the walls of the pores through the 10-4 potential;[38,39] the charge is evenly distributed over the surface of the pores. It allows us to calculate the VdW part of the electrosorption

pressure using the following equation:[43]

$$\Pi_{\mathrm{in,vdw}} = -\int_0^H \mathrm{d}z \rho(z) \frac{\mathrm{d}V_{\mathrm{ext}}}{\mathrm{d}z}, \tag{8}$$

with the derivative

$$\frac{\mathrm{d}V_{\mathrm{ext}}}{\mathrm{d}z} = 2\pi\rho_{\mathrm{s}}\Delta\sigma_{\mathrm{sf}}\epsilon_{\mathrm{sf}}\left[-4\left(\frac{\sigma_{\mathrm{sf}}}{z}\right)^{11} + 4\left(\frac{\sigma_{\mathrm{sf}}}{z}\right)^{5}\right]. \tag{9}$$

Here ρ_{s} is the volume density of carbon atoms; Δ is the interlayer distance; σ_{sf} and ϵ_{sf} are the parameters of the solid-fluid interactions determined by the Lorentz-Berthelot combining rules. Additionally, the use of Eq. 8 implies that we estimate the force in an infinitely long pore (in the x and y directions).

The electrostatic part of Π_{in} can be estimated using the pressure between two semi-infinite (infinite in the y axis but finite in the x axis) parallel planes with different widths in the x axis direction. The wider plane is located at $z = 0$ and the narrower at $z = H$, both of which are oriented perpendicular to the z axis. Using the classical results of electrostatics the final equations take the following form:

$$\Pi_{\mathrm{in,el}} = \sum_i \int_0^H P(H-z)c_i(z)\mathrm{d}z, \tag{10}$$

where i is an index running through different charge distributions, i.e. $\{\mathrm{Na}^+, \mathrm{Cl}^-, \mathrm{O}, \mathrm{H}, \xi_{\mathrm{L}}\}$ and

$$\begin{aligned} P(h) &= -\frac{\xi_{\mathrm{a}}}{2\pi\varepsilon_0}\left(\frac{h}{2a}\ln\left(\frac{h^2+(L+a)^2}{h^2+(L-a)^2}\right) + \frac{L}{a}\left[\arctan\left(\frac{L-a}{h}\right) - \arctan\left(\frac{L+a}{h}\right)\right]\right. & (11) \\ &+ \left.\arctan\left(\frac{a-L}{h}\right) - \arctan\left(\frac{a+L}{h}\right)\right), & (12) \end{aligned}$$

here by ξ_{a} and ξ_{L} we denoted the surface charge densities of the narrow and wide planes,

respectively; a and L are the widths of narrow and wide planes, respectively; h is the distance between the two planes; $P(H-z)c_i(z)\mathrm{d}z$ is the pressure contribution from the ions located at the distances between $H-z$ and $H-(z+dz)$ in the pore.

Figure 9 shows the estimations by Eqs. 8 and 10 for 1 nm and 2 nm pores, respectively. Furthermore, we added the same contributions calculated directly in MD using the last 10 ns of the production run. These calculations were performed using *rerun* LAMMPS command. As can be seen, both the electrostatic and van der Waals contributions follow a linear trend if plotted as a function of ξ^2. The estimations from the concentration profiles demonstrate qualitative agreement with the direct MD results. The only case where we also achieved quantitative agreement is the electrostatic contribution in the 2 nm pore in Fig. 9b. It suggests that the periodicity, which may affect our results, does not play a significant role in the force calculations. However, it may still affect the results through the atomic trajectories.

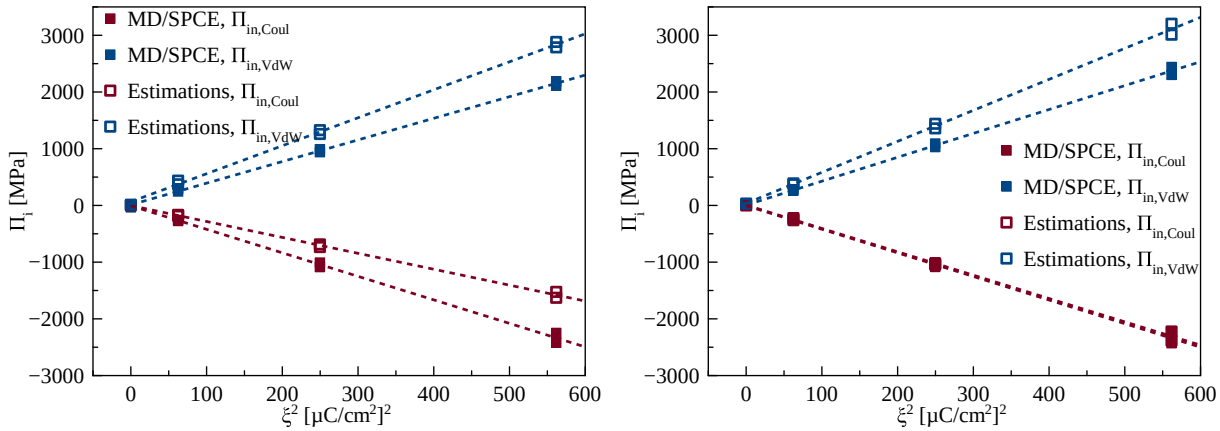

Figure 9: Estimations of the VdW and electrostatic contributions for the solvation pressure in (a) 1 nm and (b) 2 nm pores. The calculations were performed for MD/SPCE. Dotted lines represent the linear fits.

The $\Pi_{\mathrm{in,VdW}}$ estimations may also be used to study the influence of water reorientation and reorganization during pore charging. We can calculate the positive and negative contributions to the oxygen-induced part of the electrosorption pressure. Using Eq. 8 the positive contribution can be obtained only in the limited range of z coordinate from 0 to the value

where Eq. 9 turns zero, namely $z = 3.2643$. It means that the shape of the first peak in the oxygen density distribution profile defines the repulsive magnitude. So we can calculate the repulsive and attractive contributions to the nonelectrostatic part of the solvation pressure. It is instructive to compare the values at different surface charges: (509, −568) MPa and (2739,−294) MPa correspond to $\xi = 0$ and $-23.7\,\mu\mathrm{C/cm^2}$, respectively. The first value in brackets corresponds to the repulsive part of the solvation pressure, while the second one corresponds to the attractive part. The result allows us to conclude that the VdW part of the water Π_{in} is mainly affected by the narrowing of the first oxygen peak, since the positive contribution changes much more pronounced than the negative one.

Fig. 10a shows the results of the current mPB model obtained for three sets of parameters. For $\epsilon_{\mathrm{sf}} = 0\,\mathrm{K}$ we used a different equation defining solvation pressure[22] without external short-range potential:

$$P_N = P(z) - \frac{\varepsilon\varepsilon_0}{2}\left(\frac{\mathrm{d}\psi}{\mathrm{d}z}\right)^2 - P_{\mathrm{b}}, \tag{13}$$

where $P(z)$ is the ions osmotic pressure; the second term is the Maxwell stress tensor; P_{b} is the ions osmotic pressure in the bulk. An asymmetry of ion sizes or solid-ion interactions manifests itself in an asymmetry of $\Delta\Pi$. Also, as already shown in Fig. 5b, strong ion-wall short-range interactions lead to a shift in the position of the minimum solvation pressure and may result in its negative values. In the absence of solid-ion interactions, the values of $\Delta\Pi$ are significantly lower, as shown in Fig. 10b. However, the change in pore size from 2 nm to 1.5 nm significantly increases the magnitude of the solvation pressure. When the exact value of the pore width is not important or unknown, one can also rely on the modified Poisson-Boltzmann model without explicit account of additional short-range external potential, as was done in Ref.[22] for instance.

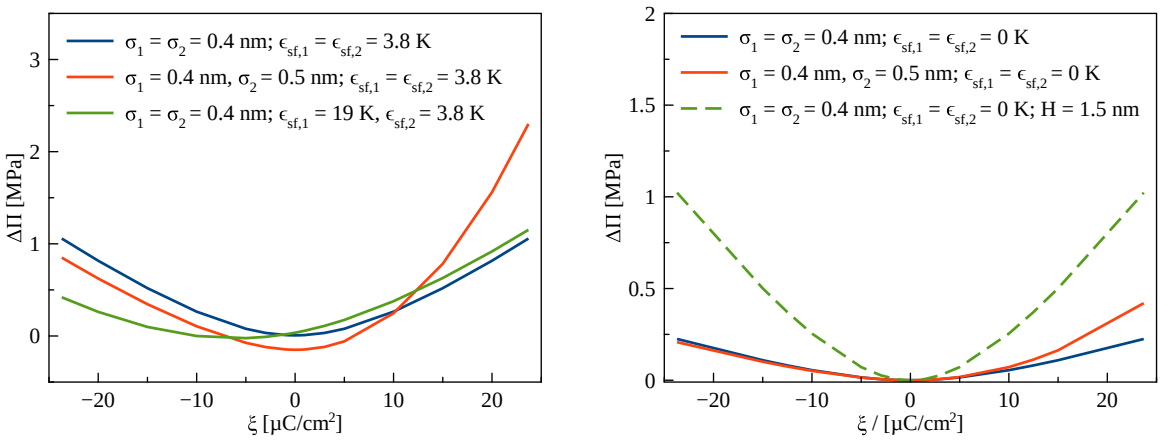

Figure 10: Solvation pressure calculated within the current mPB model using the different set of parameters given in the legend. The hard sphere diameters were calculated by Eq. 6 using $\epsilon_{\mathrm{ff}} = 50.35\,\mathrm{K}$. The pore width was set to 2 nm, unless otherwise stated.

The model developed in this work can also be used to study the deformation of microporous carbon electrodes, assuming that the main driving force of the electrosorption-induced deformation will be solvation pressure rather than surface stress.[15] Additionally, we assume that the pores have a slit geometry and that the carbon matrix itself is incompressible. The effect of pore size distribution on electrosorption-induced deformation is taken into account using the result of[44] in the discrete form:[45]

$$\frac{\Delta V_{\mathrm{sample}}}{V_{\mathrm{sample}}} = \frac{1}{M}\sum_i f_i \Delta\Pi(H_i), \tag{14}$$

where f_i is the pore volume distribution, i.e. the relative volume corresponding to the pores with width H_i; M is the effective elastic modulus of the sample; $\Delta\Pi(H_i)$ is the solvation pressure in the pores with width H_i. Our model accounts only for the pressure due to the ions; thus, we need to add a contribution from the solvent, i.e. the hydration solvation pressure. It should be noted that, in general, these two contributions are not necessary additive.[25] Also, as we showed in the **Result** section, the hydration contribution may depend on the

surface charge density. We modify the common exponential form:

$$\Delta\Pi_{\mathrm{hyd}} = (\Pi_0 + \kappa\xi^2)e^{-H/\lambda}, \tag{15}$$

where Π_0 is an amplitude at zero surface charge; κ is a coupling coefficient and λ is the decay length. However, in contrast to the hydration contribution in pure water, Eq. 15 should be treated as an effective one, due to the ion-water correlations in the EDL.[25]

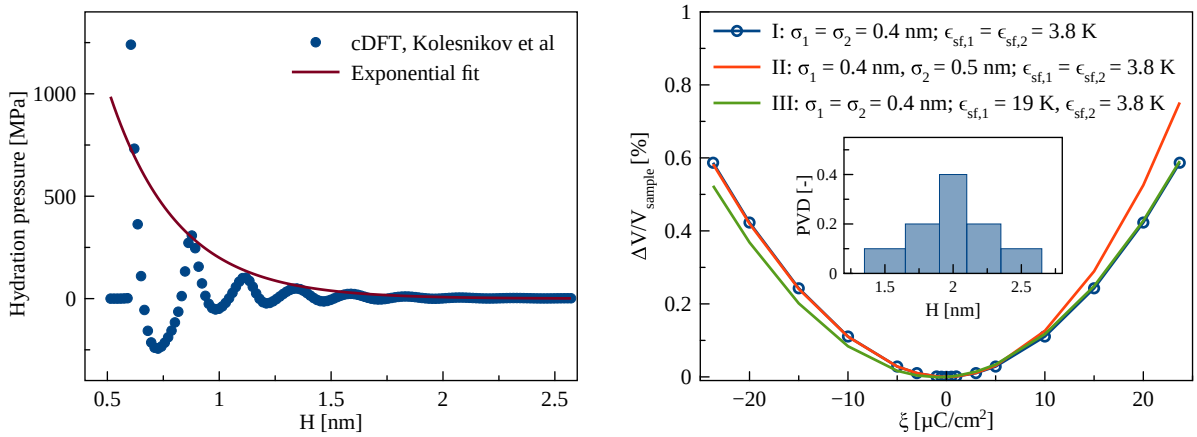

(a) (b)

Figure 11: (a) Fit of the hydration pressure calculated within the framework of classical density functional theory[46] by Eq. 15. (b) Comparison of the predicted EID for the three sets of $\varepsilon_{\mathrm{sf}}$ and σ, and the effective elastic modulus 1 GPa. Inset shows the pore volume distribution used for the averaging in Eq. 14.

To estimate the values of the parameters Π_0 and λ in Eq. 15 we used data from the literature on the solvation pressure in pure water calculated by the classical density functional theory.[46] Namely, the result corresponding to the 70° contact angle with the flat surface. This value is close to the contact angle of water on highly ordered pyrolytic graphite at 303 K[47] - 82°. The parameters were obtained from the maxima fit using Eq. 15 with $\kappa = 0$. The result is shown in Fig. 11a and the values are 5350.8 MPa and 0.3041 nm for Π_0 and λ, respectively. The value of κ was taken equal to 4.2 MPa/$(\mu\mathrm{C/cm^2})^2$ from the fit of the VdW part of the solvation pressure calculated via MD and shown in Fig. 9b.

Fig. 11b shows the theoretical prediction of electrosorption-induced deformation calculated for three sets of parameters ε_{sf} and σ (the same as in Fig. 10a), and the effective elastic modulus of 1 GPa. In our calculations, we also shifted the strain reference point to the point with zero surface charge density. The fully symmetric curve I overlaps with curve II at negative surface charges and with curve III at positive surface charges. However, the origins of the overlaps are different. At positive charges, curve III is lower than curve I due to the higher value of $\epsilon_{sf,1}$. On the other hand, curve I is lower than curve II as a result of the smaller size of the anions in that case.

Our models and molecular dynamic calculations have several limitations due to the assumptions we made. First, we calculated the solvation pressure in a finite-sized pore; thus the transition to an infinite pore may quantitatively change the MD results. Mostly, its origin should be in the electrostatic part of the solvation pressure. We can try to estimate the effect of the pore length (on the x-axis) using the concentration profiles from Fig. 3 and Eq. 10. This estimation shows that for 2 nm pore the finite-size effect is approximately 10 %. Another possible source of uncertainty could be correlations due to the effect of periodic boundary conditions on the electrostatic part of the forces or the change of Π_{out} (see Fig. 8). In the model and MD/WCA simulations we used a constant dielectric permittivity; however, this assumption could be violated in the vicinity of the interfaces.[48] Finally, as mentioned previously, our model is a local one, and its predictions gradually deteriorate with increase of ion concentrations.

Conclusion

We present a simulation study of electrosorption-induced deformation of carbonaceous materials. We focused on calculations of the solvation pressure in the graphitic pores immersed in the aqueous sodium chloride solution. Two types of simulations were performed – with explicit and implicit water models. The first one uses the SPC/E model, and in the sec-

ond one a structureless background with constant dielectric permittivity. The simulations with an implicit solvent were further used to validate the mean-field model based on the modified Poisson-Boltzmann equation, which is then utilized to predict the macroscopic electrosorption-induced deformation.

Using molecular simulations, we demonstrated two distinct behavior of the solvation pressure in 1 nm and 2 nm slit pores as a function of surface charge density. We associated the difference with the pronounced effects of molecular layering in the smaller pore. The solvation pressure behavior obtained by the continuum model in the 2 nm pore is similar to the results of the MD simulation. We demonstrated that the model can quantitatively reproduce the dependence of the solvation pressure on the pore width given by the MD simulation with implicit water. We split the solvation pressure into two contributions: short-range (included all van der Waals forces) and long-range (electrostatic forces). Our calculations showed the importance of the short-range part in compensating the attraction between the pore walls caused by long-range interactions. Furthermore, we showed that the asymmetry of electrosorption-induced deformation as a function of surface charges can have different origins. That is, a difference in the ion sizes or in the magnitude of short-range ion-wall interactions may cause the asymmetry. The current results can help to analyze the experimental data of electrosorption-induced deformation of microporous carbons. The proposed theoretical model based on the modified Poisson-Boltzmann equation can be used for predictions of electrosorption-induced deformation and may provide a basis for design carbon actuators based on this principle.

Acknowledgment

The work was supported by the National Science Foundation (CBET-2234028) and the Deutsche Forschungsgemeinschaft (DFG), (Project number 509293944), "Aqueous Electrolytes in Nanoporous Media: Structure, Dynamics and Electrochemo-Mechanical Actuation". The

authors also acknowledge the support and exchange within the research initiative BlueMat: Water-Driven Materials, Hamburg and the Centre for Molecular Water Science CMWS, Hamburg. This work used the supercomputers Wulver at the New Jersey Institute of Technology and ANVIL at Perdue University. The latter through the allocations CHM240093 and CHM240031 from the Advanced Cyber Infrastructure Coordination Ecosystem: Services & Support (ACCESS) program, which is supported by National Science Foundation grants #2138259, #2138286,#2138307, #2137603, and #2138296.[49] We thank Dr. Pedro de Souza for discussions.

References

(1) Soffer, A.; Folman, M. The electrical double layer of high surface porous carbon electrode. *Journal of Electroanalytical Chemistry and Interfacial Electrochemistry* **1972**, *38*, 25–43.

(2) Oren, Y.; Glatt, I.; Livnat, A.; Kafri, O.; Soffer, A. The electrical double layer charge and associated dimensional changes of high surface area electrodes as detected by more deflectometry. *Journal of Electroanalytical Chemistry and Interfacial Electrochemistry* **1985**, *187*, 59–71.

(3) Rochester, C. C.; Pruessner, G.; Kornyshev, A. A. Statistical mechanics of 'unwanted electroactuation' in nanoporous supercapacitors. *Electrochimica Acta* **2015**, *174*, 978–984.

(4) Augustyn, V.; Wang, R.; Balke, N.; Pharr, M.; Arnold, C. B. Deformation during Electrosorption and Insertion-Type Charge Storage: Origins, Characterization, and Design of Materials for High Power. *ACS Energy Letters* **2020**, *5*, 3548–3559.

(5) Baughman, R. H.; Cui, C.; Zakhidov, A. A.; Iqbal, Z.; Barisci, J. N.; Spinks, G. M.; Wallace, G. G.; Mazzoldi, A.; De Rossi, D.; Rinzler, A. G.; others Carbon nanotube actuators. *Science* **1999**, *284*, 1340–1344.

(6) Brinker, M.; Huber, P. Wafer-Scale Electroactive Nanoporous Silicon: Large and Fully Reversible Electrochemo-Mechanical Actuation in Aqueous Electrolytes. *Advanced Materials* **2022**, *34*, 2105923.

(7) Gómez-González, M.; Latorre, E.; Arroyo, M.; Trepat, X. Measuring mechanical stress in living tissues. *Nature Reviews Physics* **2020**, *2*, 300–317.

(8) Brinker, M.; Dittrich, G.; Richert, C.; Lakner, P.; Krekeler, T.; Keller, T. F.; Huber, N.;

Huber, P. Giant electrochemical actuation in a nanoporous silicon-polypyrrole hybrid material. *Science Advances* **2020**, *6*, eaba1483.

(9) Jain, P.; Liu, W.; Zhu, S.; Chang, C. Y.-Y.; Melkonian, J.; Rockwell, F. E.; Pauli, D.; Sun, Y.; Zipfel, W. R.; Holbrook, N. M.; Riha, S. J.; Gore, M. A.; Stroock, A. D. A minimally disruptive method for measuring water potential in planta using hydrogel nanoreporters. *Proceedings of the National Academy of Sciences of the United States of America* **2021**, *118*, e2008276118.

(10) Wang, W.; Li, J.; Liu, H.; Ge, S. Advancing versatile ferroelectric materials toward biomedical applications. *Advanced Science* **2021**, *8*, 2003074.

(11) Ahmed, A. A.; Alegret, N.; Almeida, B.; Alvarez-Puebla, R.; Andrews, A. M.; Ballerini, L.; Barrios-Capuchino, J. J.; Becker, C.; Blick, R. H.; Bonakdar, S.; others Interfacing with the Brain: How Nanotechnology Can Contribute. *ACS Nano* **2025**, *19*, 10630–10717.

(12) Weissmuller, J.; Viswanath, R.; Kramer, D.; Zimmer, P.; Wurschum, R.; Gleiter, H. Charge-induced reversible strain in a metal. *Science* **2003**, *300*, 312–315.

(13) Biener, J.; Wittstock, A.; Zepeda-Ruiz, L.; Biener, M.; Zielasek, V.; Kramer, D.; Viswanath, R.; Weissmüller, J.; Bäumer, M.; Hamza, A. Surface-chemistry-driven actuation in nanoporous gold. *Nature Materials* **2009**, *8*, 47–51.

(14) Koczwara, C.; Rumswinkel, S.; Prehal, C.; Jäckel, N.; Elsässer, M. S.; Amenitsch, H.; Presser, V.; Hüsing, N.; Paris, O. In situ measurement of electrosorption-induced deformation reveals the importance of micropores in hierarchical carbons. *ACS Applied Materials & Interfaces* **2017**, *9*, 23319–23324.

(15) Gor, G. Y.; Kolesnikov, A. L. What drives deformation of smart nanoporous materials during adsorption and electrosorption? *Langmuir* **2024**, *40*, 15949–15956.

(16) Lee, A. A.; Colby, R. H.; Kornyshev, A. A. Statics and dynamics of electroactuation with single-charge-carrier ionomers. *Journal of Physics: Condensed Matter* **2013**, *25*, 082203.

(17) Lee, A. A.; Colby, R. H.; Kornyshev, A. A. Electroactuation with single charge carrier ionomers: the roles of electrostatic pressure and steric strain. *Soft Matter* **2013**, *9*, 3767–3776.

(18) Goodwin, Z. A.; Eikerling, M.; Löwen, H.; Kornyshev, A. A. Theory of microstructured polymer–electrolyte artificial muscles. *Smart Materials and Structures* **2018**, *27*, 075056.

(19) Hansen, J.-P.; McDonald, I. R. *Theory of simple liquids: with applications to soft matter*; Academic press, 2013.

(20) Black, J. M.; Feng, G.; Fulvio, P. F.; Hillesheim, P. C.; Dai, S.; Gogotsi, Y.; Cummings, P. T.; Kalinin, S. V.; Balke, N. Strain-based in situ study of anion and cation insertion into porous carbon electrodes with different pore sizes. *Advanced Energy Materials* **2014**, *4*, 1300683.

(21) Hantel, M.; Presser, V.; Kötz, R.; Gogotsi, Y. In situ electrochemical dilatometry of carbide-derived carbons. *Electrochemistry Communications* **2011**, *13*, 1221–1224.

(22) Kolesnikov, A. L.; Mazur, D. A.; Budkov, Y. A. Electrosorption-induced deformation of a porous electrode with non-convex pore geometry in electrolyte solutions: A theoretical study. *Europhysics Letters* **2022**, *140*, 16001.

(23) Gurina, D.; Odintsova, E.; Kolesnikov, A.; Kiselev, M.; Budkov, Y. Disjoining pressure of room temperature ionic liquid in charged slit carbon nanopore: Molecular dynamics study. *Journal of Molecular Liquids* **2022**, *366*, 120307.

(24) Pellenq, R.-M.; Caillol, J.; Delville, A. Electrostatic attraction between two charged surfaces: A (N, V, T) Monte Carlo simulation. *The Journal of Physical Chemistry B* **1997**, *101*, 8584–8594.

(25) Schlaich, A.; Dos Santos, A. P.; Netz, R. R. Simulations of nanoseparated charged surfaces reveal charge-induced water reorientation and nonadditivity of hydration and mean-field electrostatic repulsion. *Langmuir* **2018**, *35*, 551–560.

(26) Van Lin, S. R.; Grotz, K. K.; Siretanu, I.; Schwierz, N.; Mugele, F. Ion-specific and ph-dependent hydration of mica–electrolyte interfaces. *Langmuir* **2019**, *35*, 5737–5745.

(27) Brekke-Svaland, G.; Bresme, F. Interactions between hydrated calcium carbonate surfaces at nanoconfinement conditions. *The Journal of Physical Chemistry C* **2018**, *122*, 7321–7330.

(28) Moreira, A.; Netz, R. Simulations of counterions at charged plates. *The European Physical Journal E* **2002**, *8*, 33–58.

(29) Kalcher, I.; Schulz, J. C.; Dzubiella, J. Electrolytes in a nanometer slab-confinement: Ion-specific structure and solvation forces. *The Journal of Chemical Physics* **2010**, *133*.

(30) Berendsen, H. J.; Grigera, J. R.; Straatsma, T. P. The missing term in effective pair potentials. *Journal of Physical Chemistry* **1987**, *91*, 6269–6271.

(31) Malmberg, C.; Maryott, A. Dielectric Constant of Water from 00 to 1000 C. *Journal of research of the National Bureau of Standards* **1956**, *56*, 1–8.

(32) Weeks, J. D.; Chandler, D.; Andersen, H. C. Role of repulsive forces in determining the equilibrium structure of simple liquids. *The Journal of Chemical Physics* **1971**, *54*, 5237–5247.

(33) Smith, D. E.; Dang, L. X. Computer simulations of NaCl association in polarizable water. *The Journal of Chemical Physics* **1994**, *100*, 3757–3766.

(34) Moučka, F.; Nezbeda, I.; Smith, W. R. Molecular force fields for aqueous electrolytes: SPC/E-compatible charged LJ sphere models and their limitations. *The Journal of Chemical Physics* **2013**, *138*.

(35) Cheng, A.; Steele, W. Computer simulation of ammonia on graphite. I. Low temperature structure of monolayer and bilayer films. *The Journal of Chemical Physics* **1990**, *92*, 3858–3866.

(36) Ben-Yaakov, D.; Andelman, D.; Harries, D.; Podgornik, R. Beyond standard Poisson–Boltzmann theory: ion-specific interactions in aqueous solutions. *Journal of Physics: Condensed Matter* **2009**, *21*, 424106.

(37) Budkov, Y. A.; Kolesnikov, A. L. Modified Poisson–Boltzmann equations and macroscopic forces in inhomogeneous ionic fluids. *Journal of Statistical Mechanics: Theory and Experiment* **2022**, *2022*, 053205.

(38) Siderius, D. W.; Gelb, L. D. Extension of the Steele 10-4-3 potential for adsorption calculations in cylindrical, spherical, and other pore geometries. *The Journal of Chemical Physics* **2011**, *135*.

(39) Kowalczyk, P.; Ciach, A.; Neimark, A. V. Adsorption-induced deformation of microporous carbons: Pore size distribution effect. *Langmuir* **2008**, *24*, 6603–6608.

(40) Rosenfeld, Y. Free-energy model for the inhomogeneous hard-sphere fluid mixture and density-functional theory of freezing. *Physical Review Letters* **1989**, *63*, 980.

(41) Roth, R. Fundamental measure theory for hard-sphere mixtures: a review. *Journal of Physics: Condensed Matter* **2010**, *22*, 063102.

(42) Kolafa, J.; Nezbeda, I. The Lennard-Jones fluid: an accurate analytic and theoretically-based equation of state. *Fluid Phase Equilibria* **1994**, *100*, 1–34.

(43) Balbuena, P. B.; Berry, D.; Gubbins, K. E. Solvation pressures for simple fluids in micropores. *The Journal of Physical Chemistry* **1993**, *97*, 937–943.

(44) Kowalczyk, P.; Ciach, A.; Neimark, A. V. Adsorption-induced deformation of microporous carbons: Pore size distribution effect. *Langmuir* **2008**, *24*, 6603–6608.

(45) Kolesnikov, A. L.; Möllmer, J. Temperature Evolution of Sorbonorit-4 Methane-Induced Deformation through the Eyes of Classical Density Functional Theory. *Langmuir* **2024**, *40*, 4122–4131.

(46) Kolesnikov, A.; Budkov, Y.; Barbosa, G.; Möllmer, J.; Tavares, F. Water adsorption on planar interfaces: Classical density functional study. *Fluid Phase Equilibria* **2023**, *564*, 113567.

(47) Friedman, S. R.; Khalil, M.; Taborek, P. Wetting transition in water. *Physical Review Letters* **2013**, *111*, 226101.

(48) Fumagalli, L.; Esfandiar, A.; Fabregas, R.; Hu, S.; Ares, P.; Janardanan, A.; Yang, Q.; Radha, B.; Taniguchi, T.; Watanabe, K.; others Anomalously low dielectric constant of confined water. *Science* **2018**, *360*, 1339–1342.

(49) Boerner, T. J.; Deems, S.; Furlani, T. R.; Knuth, S. L.; Towns, J. Access: Advancing innovation: NSF's advanced cyberinfrastructure coordination ecosystem: Services & support. Practice and Experience in Advanced Research Computing 2023: Computing for the Common Good. **2023**, 173–176.